Title
Aquaporin-4 regulates the velocity and frequency of cortical spreading depression in mice.

Journal
Glia, 63(10)

ISSN
0894-1491

Authors
Yao, Xiaoming
Smith, Alex J
Jin, Byung-Ju
et al.

Publication Date
2015-10-01

DOI
10.1002/glia.22853

Peer reviewed

HHS Public Access

Author manuscript

Glia. Author manuscript; available in PMC 2016 October 01.

Published in final edited form as:

Glia. 2015 October ; 63(10): 1860–1869. doi:10.1002/glia.22853.

Aquaporin-4 Regulates the Velocity and Frequency of Cortical Spreading Depression in Mice

Xiaoming Yao[1,2], **Alex J. Smith**[1], **Byung-Ju Jin**[1], **Zsolt Zador**[2], **Geoffrey T. Manley**[2], and **A.S. Verkman**[1]

[1]Department of Medicine and Physiology, University of California, San Francisco, CA 94143, USA

[2]Department of Neurological Surgery, University of California, San Francisco, CA 94143, USA

Abstract

The astrocyte water channel aquaporin-4 (AQP4) regulates extracellular space (ECS) K^+ concentration ($[K^+]_e$) and volume dynamics following neuronal activation. Here, we investigated how AQP4-mediated changes in $[K^+]_e$ and ECS volume affect the velocity, frequency and amplitude of cortical spreading depression (CSD) depolarizations produced by surface KCl application in wild-type ($AQP4^{+/+}$) and AQP4-deficient ($AQP4^{-/-}$) mice. Contrary to initial expectations, both the velocity and frequency of CSD were significantly reduced in $AQP4^{-/-}$ mice when compared to $AQP4^{+/+}$ mice, by 22% and 32%, respectively. Measurement of $[K^+]_e$ with K^+-selective microelectrodes demonstrated an increase to ~35 mM during spreading depolarizations in both $AQP4^{+/+}$ and $AQP4^{-/-}$ mice, but the rates of $[K^+]_e$ increase (3.5 vs. 1.5 mM/s) and reuptake ($t_{1/2}$ 33 vs. 61 s) were significantly reduced in $AQP4^{-/-}$ mice. ECS volume fraction measured by trimethylammonium iontophoresis was greatly reduced during depolarizations from 0.18 to 0.053 in $AQP4^{+/+}$ mice, and 0.23 to 0.063 in $AQP4^{-/-}$ mice. Analysis of the experimental data using a mathematical model of CSD propagation suggested that the reduced velocity of CSD depolarizations in $AQP4^{-/-}$ mice was primarily a consequence of the slowed increase in $[K^+]_e$ during neuronal depolarization. These results demonstrate that AQP4 effects on $[K^+]_e$ and ECS volume dynamics accelerate CSD propagation.

Keywords

AQP4; CSD; extracellular space; potassium; astrocyte

INTRODUCTION

Aquaporin-4 (AQP4) is a bidirectional, water-selective transport protein expressed at the plasma membrane of astrocytes throughout the central nervous system (Frigeri et al. 1995; Nielsen et al. 1997), where it increases water permeability of the astrocyte plasma membrane (Solenov et al. 2004) and of the blood-brain barrier (Papadopoulos et al. 2004; Papadopoulos and Verkman 2005; Thiagarajah et al. 2005). Phenotype studies of AQP4-deficient ($AQP4^{-/-}$) mice have provided evidence for the involvement of AQP4 in brain

Address correspondence to: Xiaoming Yao, M.D., Ph.D., 1246 Health Sciences East Tower, University of California San Francisco, CA 94143-0521, U.S.A. Phone 415 476-8530; Fax 415 665-3847; xiaoming.yao@ucsf.edu.

water balance, astrocyte migration and regulation of neuronal excitability (Papadopoulos and Verkman 2013). AQP4$^{-/-}$ mice manifest several indications of altered excitability, including increased seizure threshold (Binder et al. 2004) and prolonged seizure duration (Binder et al. 2006); a similar seizure phenotype was found in α-syntrophin knockout mice in which there is secondary AQP4 deficiency owing to defective AQP4 plasma membrane targeting (Amiry-Moghaddam et al. 2003). AQP4$^{-/-}$ mice also show impaired electrophysiological and/or behavioral responses to auditory (Li and Verkman 2001), visual (Li et al. 2002) and olfactory (Lu et al. 2008) stimuli.

Altered $[K^+]_e$ dynamics in AQP4 deficiency is associated with, and perhaps causes, the neuroexcitation phenotypes in AQP4$^{-/-}$ mice. *In vivo* and brain slice studies have shown slowed accumulation of K^+ during neuroexcitation (Binder et al. 2006; Strohschein et al. 2011) in AQP4$^{-/-}$ mice, and slowed clearance of K^+ from the ECS following neuroexcitation (Padmawar et al. 2005; Strohschein et al. 2011). Colocalization and physical association studies (Amiry-Moghaddam et al. 2004; Connors et al. 2004; Connors and Kofuji 2006; Kofuji and Newman 2004) have suggested that interaction of AQP4 with the inwardly rectifying K^+ channel Kir4.1 might account for altered ECS K^+ dynamics in AQP4 deficiency; however, patch-clamp studies in brain astrocytes and retinal Muller cells did not show effects of AQP4 expression on Kir4.1 K^+ conductance (Ruiz-Ederra et al. 2007; Zhang and Verkman 2007). We subsequently proposed a mechanism, based on coupled K^+/water uptake by astrocytes following neuronal K^+ release, in which basal ECS volume expansion and reduced astrocyte water permeability in AQP4$^{-/-}$ mice could account for altered ECS K^+ dynamics (Jin et al. 2013).

Here, the role of AQP4 in neuroexcitation was further studied utilizing a robust model of neuroexcitation in live mice – cortical spreading depression (CSD), in which large increases in ECS K^+ concentration and reductions in ECS volume occur during spatially propagating waves of cortical depolarization (Kume-Kick et al. 2002; Sykova and Nicholson 2008). CSD is the cause of migraine aura and shares many mechanistic features with spreading depolarizations that contribute to lesion development following ischemia (Pietrobon and Moskowitz 2014). Earlier work from our lab using a K^+-sensing fluorescent dye showed altered ECS K^+ dynamics in AQP4$^{-/-}$ mice during CSD produced by mechanical pinprick (Padmawar et al. 2005). Using electrophysiological methods here we report slowed CSD wave velocity and frequency in AQP4$^{-/-}$ mice, and investigated potential mechanisms by measurements of ECS K^+ and volume during CSD, and mathematical modeling of CSD propagation velocity.

MATERIALS AND METHODS

AQP4$^{-/-}$ mice

AQP4$^{-/-}$ mice in a CD1 genetic background were generated as described (Ma et al. 1997). These mice lack detectable AQP4 protein, and show normal growth, development, survival, and neuromuscular function, and no gross or microscopic differences in the anatomy of the nervous system or vasculature (Manley et al. 2000). All animal procedures were performed with an approved protocol from the UCSF Committee on Animal Research.

In vivo preparation

Mice were anesthetized using 2.5% Avertin (2,2,2-tribromoethanol, 250 mg/kg, i.p., Sigma-Aldrich, St. Louis, MO) and immobilized in a stereotaxic apparatus. Additional Avertin (85 mg/kg) was administered every hour to maintain anaesthesia. The mice breathed room air spontaneously and body temperature was maintained at 37 ± 0.5 °C using a heating pad. All measurements were made within 1–3 hours after surgery. The aCSF solution contained (in mM): 126 NaCl, 3 KCl, 26 $NaHCO_3$, 1.25 NaH_2PO_4, 10 D-glucose, 1.3 $MgCl_2$, 1.5 $CaCl_2$, gassed with 95% O_2/5% CO_2 to buffer pH at 7.4. TMA-chloride (0.5 mM) was added for TMA^+ calibrations.

For induction of CSD and measurement of DC potential and $[K^+]_e$, three 1-mm diameter burr holes were made 1.5 mm to the right of the midline, and positioned +2 mm, −0.5 mm and −3 mm from bregma. These holes were used for CSD induction (by 1M KCl application), and DC potential and $[K^+]_e$ recording (at site-1 and site-2) using double-barreled electrodes. A ground wire was attached to the skull and also grounded to a Faraday cage. For TMA^+ measurements the skull was exposed by midline skin incision, an atraumatic craniectomy was made over the somatosensory cortex (1.5 mm lateral and 1.5 mm caudal to bregma), and the dura was carefully removed (Yao et al. 2008). The skin flaps were held open with a cylindrical plastic dam (13 mm diameter and 4 mm height) and aCSF at 37 °C was superfused over the brain at 2 ml/min. A small plastic container (4-mm diameter and 5-mm height) was glued to the inner wall of the dam to hold agarose gel for control measurements.

CSD induction

Recurrent CSD was elicited by epidural application of 1M KCl for one hour (Godukhin and Obrenovitch 2001) using a high-precision syringe pump (KD Scientific Inc., MA) connected to a small pulled glass fiber (450 μm outer diameter x 320 μm inner diameter) positioned with a stereotactic arm just above the exposed dura. CSD was initiated with KCl application to the dura at 1 μl/min and then reduced to 0.15 μl/min for the duration of the experiment. This procedure reproducibly induced characteristic CSD waves in mice. The application of KCl remained restricted to the small area of exposed dura, with no lateral diffusion between bone and dura. Removal of the glass fiber and extensive rinsing with saline terminated the CSD.

DC and $[K^+]_e$ measurement using K^+ ion-sensitive microelectrodes

K^+ ion-selective microelectrodes (K^+-ISM) were pulled from double-barrelled theta-glass (Cat. No. 64-0811, Warner Instruments, Hamden, CT) with a final O.D. of 2–5 μm, and fabricated as described (Nicholson 1993; Prince et al. 1973). The liquid K^+-ion exchanger Fluka Ionophore-Cocktail A (FCat. # 60031, Fluka, St. Louis, MO) was filled in the ion-sensing barrel, and backfilled with 100 mM KCl. Another barrel was filled with 150 mM NaCl and served as a reference electrode for subtraction of cortical DC potential using a dual-channel microelectrode preamplifier (Model IX2-700; Dagan Corp., Minneapolis, MN). Each ISM was calibrated before and after the experiment using K^+ solution standards (1, 3, 5, 10, 30, 50 and 100 mM KCl); data were included in the analysis only when calibrations before and after the experiment were in the same range. An MP150 amplifier

(Biopac, Goleta, CA) was used for online digital sampling. Voltage data were converted into K^+ concentration using least squares non-linear regression. Electrodes were not used for this study unless there was at least a 50 mV change between the 3 mM and 30 mM K^+ standards, though this relatively small changes in voltage (60 mV for ideal electrode) may be related to the low input impedance of the amplifier.

DC potentials and $[K^+]_e$ were measured simultaneously in the anterior two burr holes (site 1 and site-2). ISMs were placed 400 μm below the surface of the cortex. Absolute DC amplitude (in mV) and CSD frequency (number of CSD depolarization per hour of recording) were measured. The velocity of CSD wave propagation across the cortex was determined from the time for the CSD wave to propagate from site-1 to site-2 (2.5 mm apart in the anterior-posterior direction). The rate of K^+ release (in mM/s) was determined by linear regression; half-time ($t_{1/2}$, in s^{-1}) for K^+ recovery to baseline ('K^+ clearance') was calculated by exponential regression using GraphPad Prism software.

ECS volume and diffusion measurement using TMA^+ ion-sensitive microelectrodes

Microelectrodes for iontophoretic delivery and TMA^+- ion-selective microelectrodes (ISMs) were both pulled from double-barrelled theta-glass (Cat. No. 64-0811, Warner Instruments, Hamden, CT) with a final outer diameter of 2–5 μm, and fabricated as described (Dietzel et al. 1980; Nicholson 1993). A tetraphenylborate-based ion exchanger (Corning 477317, currently available as IE190 from WPI, Sarasota, FL) was used in the ion-sensing barrel, which was backfilled with 150 mM TMA-Cl using a 10-mm high column (Neher and Lux 1973). The reference barrel contained 150 mM NaCl. To extract the TMA^+ signal, the voltage measured by the reference barrel was subtracted from the voltage measured by the ion-detecting barrel using a dual-channel microelectrode preamplifier (Model IX2-700; Dagan Corp., Minneapolis, MN). Each extracellular microelectrode was calibrated in solutions containing 0.5, 1, 2, 4 and 8 mM TMA-Cl in 150 mM NaCl, using the Nikolsky equation. The iontophoresis microelectrode contained 150 mM TMA-Cl.

For *in vivo* diffusion measurements, the shank of the iontophoretic microelectrode was bent and aligned parallel with the extracellular microelectrode, and glued together using dental cement with an inter-tip distance of 50–100 μm, as described (Yao et al. 2008). Control TMA^+ diffusion curves were first recorded in agarose gel (0.3% NuSieve GTG, FMC BioProducts, Rockland, ME) in 150 mM NaCl and 0.5 mM TMA-Cl to obtain the transport number n_t of the iontophoresis microelectrode and confirm the microelectrode spacing r, then measurements were made in brain to obtain the apparent diffusion coefficient D^*, α, λ, and the constant k' that accounted for non-specific loss of TMA^+ from the ECS. A constant bias current of +20 nA was applied to the iontophoresis microelectrode from a high-impedance source (model ION-100, Dagan Corp., Minneapolis, MN) to maintain a stable n_t (Nicholson and Phillips 1981). To generate a diffusion curve, an additional 100 nA iontophoretic current pulse was applied for 6 s. The subtracted ion and reference signals were amplified and low-pass filtered (4 Hz) using a CyberAmp 380 (Axon-CNS, Molecular Devices, Sunnyvale, CA). Diffusion curves were digitized and recorded for conversion to TMA^+ concentration using calibration data, as described (Hrabětová and Nicholson 2007). The electrode array was aligned along a transverse axis at a depth of 400 μm in the

somatosensory neocortex where it is isotropic (Lehmenkuhler et al. 1993) so that measurement along a single axis suffices to determine α, λ and k'. To verify the constancy of the transport number n_t of the iontophoresis microelectrode and confirm the microelectrode spacing r, additional measurements were made in a dilute 0.3% agarose gel in 150 mM NaCl and 0.5 mM TMA-Cl after the brain diffusion experiments.

Membrane fractionation and immunoblot anlaysis

Membrane fractions from whole brains of $AQP4^{+/+}$ and $AQP4^{-/-}$ mice were prepared as described (Ma et al. 1997). Brain was homogenized in PBS (pH 7.4) containing 250 mM sucrose and 20 μg/ml PMSF. The homogenate was centrifuged at 1000g for 10 min at 4 °C, and the supernatant was adjusted to 1.4 M sucrose solution in PBS (pH 7.4). A discontinuous sucrose density gradient [2 M sucrose (0.5 ml), 1.6 M (0.9 ml), 1.4 M (1.8 ml, containing homogenate), 1.2 M (1.8 ml), 0.8 M (0.5 ml)] was created and centrifuged at 4 °C for 2.5 hours at 25,000 rpm. After centrifugation, the top of the gradient containing the membrane fraction was collected and used for immunoblot analysis. Proteins were resolved using 12% or 5–20% polyacrylamide gels, and electrotransferred onto membranes (Amersham, Pescataway, NJ) overnight at 20 V. Membranes were blocked with 3% albumin for 1 h, and then incubated with a 1:1000 of AQP4 (Chemicon, Temecula, CA), 1:200 of α-syntrophin (Santa Cruz Biotechnology), 1:400 of Kir4.1 (Alomone Labs, Jerusalem, Israel) or 1 μg/ml for Cx43 (Chemicon) rabbit polyclonal antibodies, or 1:2000 GAPDH mouse monoclonal antibody (Chemicon). Proteins were visualized using the ECL system (Amersham).

Immunofluorescence

Brain sections were prepared as described (Oshio et al. 2004). Briefly, after blocking at room temperature for 1 h in blocking buffer (5% NGS in PBS for AQP4 and α-syntrophin, 10% NDS in PBS for Kir4.1 and Cx43), 14-μm thick sections were incubated with primary antibody at 4 °C overnight (anti-AQP4, 1:400 in 1% NGS/PBS; anti-Kir4.1, 1:100 in 1% NDS/1% BSA/PBS; anti-Cx43 1:250 in 0.3% Triton X-100/PBS). Following washing, sections were incubated with secondary antibody (rhodamine Red-X, anti-rabbit IgG, 1:200, Vector Laboratories). Immunofluorescence was examined with Nikon (Melville, NY) laser-scanning confocal microscope.

Mathematical modelling

CSD propagation velocity was modelled in Matlab as described by Zandt et al. (Zandt et al. 2013). The model required four parameters. The rate constant for K^+ reuptake was calculated from an exponential fit to the relaxation phase of the experimentally measured $[K^+]_e$. The K^+ release rate was determined from the linear slope of the $[K^+]_e$ increase during CSD, corrected for the predicted K^+ removal rate at 20 mM $[K^+]_e$. The effective K^+ diffusion coefficient was calculated from the diffusion coefficient of K^+ in water corrected for temperature and the measured extracellular tortuosity.

Statistics

Data are expressed as mean ± SEM. The significance of differences between experimental groups was determined by one-way ANOVA. Differences were regarded as statistically significant at $P < 0.05$. Analysis was performed using SPSS (Chicago, IL) and Graphpad Prism (La Jolla, CA) statistical software.

RESULTS

AQP4-depedent CSD wave amplitude, propagation velocity and frequency

Repetitive CSD waves of cortical depolarization were produced in $AQP4^{+/+}$ and $AQP4^{-/-}$ mice by epidural application of 1M KCl. DC potential was recorded simultaneously at two cortical sites located in the motor and somatosensory cortex, anterior to the site of KCl application (Figure 1A). Stable DC potential recordings over at least one hour were obtained in all mice. Representative DC potential recordings during CSD are shown over ~20 min in Figure 1B (left panel). KCl application produced a characteristic series of cortical depolarizations (CSD episodes), with lower frequency in $AQP4^{-/-}$ than $AQP4^{+/+}$ mice. The propagation velocity of the depolarization wave was determined from the delay in appearance of CSD waves at site-2 compared with site-1. As seen on an expanded time-scale, CSD wave propagation velocity was lower in $AQP4^{-/-}$ than $AQP4^{+/+}$ mice (dashed lines, Figure 1B, right panel) and wave shape was broader.

Figure 1C summarizes CSD wave amplitude, width at half-maximum, propagation velocity, and frequency (8 mice per genotype). There was a small but significant ~11% reduction in $AQP4^{-/-}$ compared to $AQP4^{+/+}$ mice in CSD wave amplitude (19.6 ± 1.4 vs. 22.0 ± 1.8 mV, n = 8 per group) and increase in width. CSD wave propagation velocity was ~22% lower (2.9 ± 0.1 vs. 3.7 ± 0.1 mm/min, n = 8 per group), and frequency was remarkably reduced by ~32% (6.9 ± 0.3 vs. 10.2 ± 0.5 CSDs/h, n = 8 per group) in $AQP4^{-/-}$ compared to $AQP4^{+/+}$ mice. These results support a role of AQP4 in CSD wave initiation and propagation, which is examined mechanistically below.

Extracellular space potassium dynamics during CSD

K^+-sensitive microelectrodes were used to investigate the effect of AQP4 deletion on ECS K^+ ($[K^+]_e$) dynamics during CSD induced by KCl application. Before and after each experiment the double-barreled K^+-sensitive microelectrodes were calibrated in K^+ solution standards as shown in Figure 2A in order to convert voltage data into $[K^+]_e$ values. DC potential and $[K^+]_e$ were recorded simultaneously as seen in the representative curves in Figure 2B from three $AQP4^{+/+}$ and $AQP4^{-/-}$ mice. KCl application produced depolarization accompanied by a large increase in $[K^+]_e$, characteristic of CSD. Curve shape differed between the $AQP4^{+/+}$ and $AQP4^{-/-}$ mice, with most noticeably a slower return of $[K^+]_e$ to baseline in the $AQP4^{-/-}$ mice.

During CSD, $[K^+]_e$ was measured at a depth of 400 μm in the somatosensory cortex (1.5 mm lateral and 1.5 mm caudal to Bregma), which was approximately 2.5 mm away from the site where SD was induced. $[K^+]_e$ kinetics during CSD was quantified as the rate of initial increase in $[K^+]_e$ (in mM/s, 'K^+ release'), and the exponential time constant for recovery to

baseline (in s^{-1}, 'K^+ clearance'), as summarized in Figure 2C (left). The rate of K^+ release was reduced by ~57% in $AQP4^{-/-}$ compared to $AQP4^{+/+}$ mice, and the time constant for K^+ clearance was increased by ~87%. There was no significant difference in baseline (2.60 ± 0.09 vs. 2.40 ± 0.07 mM) or peak $[K^+]_e$ (34.3 ± 0.8 vs. 35.5 ± 0.7 mM) in $AQP4^{+/+}$ and $AQP4^{-/-}$ mice (Figure 2C, right). The slowed K^+ kinetics in $AQP4^{-/-}$ mice supports the involvement of AQP4 in ECS K^+ homeostasis.

Extracellular space volume changes during CSD

ECS volume and diffusion parameters were measured *in vivo* in the cerebral cortex of $AQP4^{+/+}$ and $AQP4^{-/-}$ mice before, during and after CSD induced by 1M KCl. The TMA^+ method was used in which TMA^+ is introduced through a micropipette by iontophoresis and TMA^+ concentration at a small distance away from the introduction site is measured using a TMA^+-selective microelectrode (Figure 3A). Figure 3B shows representative recordings of TMA^+ microelectrode potential and DC potential in $AQP4^{+/+}$ and $AQP4^{-/-}$ mice before, during and after CSD. Figure 3C shows the kinetics of deduced TMA^+ concentration; the non-zero baseline TMA^+ concentration (average 0.78 mM) is due to the slow continuous TMA^+ iontophoresis between pulses, and the different curve shapes compared to the TMA^+ microelectrode potential in Figure 3B is due to the logarithmic relationship between TMA^+ potential and concentration. Figure 3D summarizes deduced α and λ values, showing greatly reduced α and increased λ during CSD, as well as a ~30% baseline ECS expansion in $AQP4^{-/-}$ compared to $AQP4^{+/+}$ mice.

Expression of AQP4-related proteins in $AQP4^{+/+}$ and $AQP4^{-/-}$ mouse brain

AQP4 is coexpressed in astrocytes with the inwardly-rectifying K^+ channel, Kir4.1 (Nagelhus et al. 1999), as well as adaptor protein α-syntrophin, which has been proposed to interact with a putative AQP4/Kir4.1 complex (Neely et al. 2001). Immunofluorescence in Figure 4A shows AQP4 expression in cortex of $AQP4^{+/+}$ mice, which was absent in $AQP4^{-/-}$ mice. The expression patterns of Kir4.1 and α-syntrophin were similar in $AQP4^{+/+}$ and $AQP4^{-/-}$ mice, as was the pattern of expression of astrocyte gap junction protein, connexin-43 (Cx43), which had the expected punctate pattern. Protein amounts in a membrane fraction of whole brain homogenates were quantified by immunoblot analysis (Figure 4B). A band corresponding to AQP4 was seen in membrane fractions of $AQP4^{+/+}$ but not $AQP4^{-/-}$ mice. Bands at the expected molecular sizes were seen for Kir4.1, α-syntrophin and Cx43 were seen using their respective antibodies. By densitometry, AQP4 deletion did not alter the expression of these proteins (Figure 4C).

Computational modelling of CSD propagation velocity

Propagation of waves of spreading depression requires an increase in ECS K^+ concentration to depolarize neurons and cause additional K^+ release. Recently, Zandt et al. (Zandt et al. 2013) reported a model of the initiation and propagation of cortical spreading depression using four parameters: a concentration threshold for neuronal depolarization, the K^+ release rate, the K^+ removal rate, and the effective tissue diffusion coefficient for K^+. In $AQP4^{-/-}$ mice both the release and removal rate of K^+ are slowed (Figure 2C) and the effective diffusion coefficient for K^+ is slightly increased due to the small reduction in extracellular

tortuosity observed in AQP4$^{-/-}$ mice (Figure 3D). The K^+ concentration threshold for neuronal depolarization is not expected to vary between AQP4$^{+/+}$ and AQP4$^{-/-}$ mice.

We applied model of Zandt et al. (Zandt et al. 2013) to our data to determine if the reduced CSD propagation velocity observed in AQP4$^{-/-}$ mice could be predicted by the experimentally measured changes in K^+ release rate, K^+ removal rate and extracellular tortuosity. Model results demonstrated a slower increase in $[K^+]_e$ in AQP4$^{-/-}$ than in AQP4$^{+/+}$ mice (Figure 5A), which predicted a slowed CSD propagation velocity (0.95 vs. 1.32 mm/min). This difference is the consequence of the sensitivity of CSD velocity to changes in release rate around the experimentally observed values, and the relative insensitivity to changes in the reuptake rate (Figure 5B). Changes in the effective extracellular diffusion coefficient or in the threshold K^+ concentration for neuronal depolarization, the two other model parameters, altered absolute CSD velocity but had little effect on the relative CSD velocity in AQP4$^{+/+}$ vs. AQP4$^{-/-}$ mice (Figure 5C), demonstrating the robustness of the conclusion. Modeling results therefore demonstrate that the reduced CSD propagation velocity in AQP4$^{-/-}$ mice is explicable on the basis of the reduced rate of increase in $[K^+]_e$.

DISCUSSION

We investigated the effect of AQP4 deletion on the propagation of depolarization waves, $[K^+]_e$ dynamics, and ECS volume during CSD. Repetitive CSD occurred in response to sustained cortical KCl application, with characteristic large elevations in ECS K^+ concentration and reductions in ECS volume. The major experimental findings were significantly reduced velocity, frequency and amplitude of CSD depolarization in AQP4$^{-/-}$ compared to AQP4$^{+/+}$ mice, slowed increase of ECS K^+ concentration during individual depolarization, and slowed return to baseline. ECS volume fraction was greatly and similarly reduced and tortuosity increased during depolarization in the AQP4$^{+/+}$ and AQP4$^{-/-}$ mice. The differences in K^+ dynamics could not be accounted for by differences in the expression of Kir4.1, α-syntrophin or connexin-43 in AQP4$^{+/+}$ versus AQP4$^{-/-}$ mice. Mathematical modeling utilizing experimentally determined model parameters supported the conclusion that reduction in the rate of $[K^+]_e$ increase could account for the reduced CSD propagation velocity in AQP4$^{-/-}$ mice.

Initiation and propagation of CSD requires depolarization-dependent release of neuronal K^+ into the ECS. If sufficient K^+ reaches adjacent neurons, causing depolarization and further K^+ release, the process repeats and a wave of depolarization spreads across the cortex (Grafstein 1956; Leao 1944; Somjen 2001). The increase in $[K^+]_e$ is countered by K^+ uptake and redistribution by astrocytes and by diffusion in the ECS. Changes in K^+ distribution during CSD are associated with cell swelling and a consequent substantial reduction in ECS volume (Hansen and Olsen 1980; Jing et al. 1994). Changes in $[K^+]_e$ and ECS volume promote K^+ clearance; K^+ elevation causes osmotic swelling of astrocytes, which increases the rate of K^+ uptake (Haj-Yasein et al. 2012; Jin et al. 2013). AQP4 expression increases the rate of osmotic swelling in cortical astrocytes 7-fold (Solenov et al. 2004); the rate of K^+ clearance is reduced in AQP4$^{-/-}$ mice both in response to physiological stimulation (Haj-Yasein et al. 2012) and in CSD (Padmawar et al. 2005; Thrane et al. 2013). In addition to a

swelling-dependent role, AQP4 participation in K^+ siphoning through glial end-feet has been proposed (Nagelhus et al. 1999). Here, we found greatly slowed K^+ clearance following CSD in AQP4$^{-/-}$ mice despite similar reduction in ECS volume at the peak of the CSD wave, suggesting that AQP4 might participate in swelling-independent K^+ clearance mechanisms in response to the large K^+ loads produced during CSD. Regardless of mechanism, decreased K^+ clearance by itself would be expected to increase CSD propagation velocity, so the observed decrease in velocity in AQP4$^{-/-}$ must be the consequence of other factors.

ECS K^+ diffusion is generally considered an important determinant of CSD velocity (Pietrobon and Moskowitz 2014). We found here that the tortuosity for TMA^+ was increased to similar levels in both AQP4$^{+/+}$ and AQP4$^{-/-}$ mice during CSD (Figure 3D). Therefore, the difference in CSD propagation velocity between AQP4$^{+/+}$ and AQP4$^{-/-}$ mice is not due to differences in the complexity of the extracellular diffusional path. K^+ is also redistributed throughout the gap-junction coupled astrocyte syncytium, and recent studies have found increased tracer dye coupling of hippocampal astrocytes and increased intercellular redistribution of K^+ in AQP4$^{-/-}$ mice (Strohschein et al. 2011). The role of intercellular gap junction coupling during the propagation of spreading depression is controversial; studies using pharmacological gap junction inhibitors have reported inhibition of spreading depression (Nedergaard et al. 1995), biphasic, dose-dependent effects (Martins-Ferreira and Ribeiro 1995) or accelerated propagation (Tamura et al. 2011). Genetic ablation of connexin-43 in astrocytes reduces intercellular coupling and accelerates propagation of hippocampal spreading depression (Theis et al. 2003). It is therefore possible that increased intercellular astrocyte coupling may contribute to slowing of CSD propagation in AQP4$^{-/-}$ mice; however, we did not detect major changes in the expression or localization of proteins putatively involved in spatial redistribution of K^+ through astrocytes, suggesting that these mechanisms are not drastically altered in AQP4$^{-/-}$ mice.

Mathematical models of different levels of sophistication have been used to describe various aspects of CSD propagation (Miura et al. 2013). Recently, Zandt et al. (Zandt et al. 2013) reported that a simplified model of K^+ release, diffusion and reuptake could largely explain experimentally measured CSD propagation rates. Application of this model to our experimental data recapitulated findings of reduced CSD propagation rate in AQP4$^{-/-}$ and supported the conclusion that the rate of K^+ release is the key determinant of propagation velocity. Our experimental and theoretical results suggest that slowing of the initial rate of $[K^+]_e$ increase in AQP4 deficiency, as a result of increased basal ECS volume fraction and reduced initial swelling rate, is the primary cause of the observed reduction in CSD propagation velocity. Consistent with this hypothesis, CSD propagation velocity is slowed in anesthetized versus awake animals (Guedes and Barreto 1992), where extracellular volume fraction is also increased (Xie et al. 2013). Although we did not explicitly model the effect of AQP4 deletion on the frequency of CSD waves in response to continual KCl application, similar considerations likely apply to the initiation of CSD as to its propagation.

Several caveats and limitations of our study should be noted. The methodology used to measure tortuosity during spreading depression is subject to inaccuracies because of the continuously changing ECS size during the CSD wave (Mazel et al. 2002). The short

iontophoretic pulses thus allowed only an estimation the diffusion parameters from the fitted data during SD, though we tried to minimize the error by using a smaller tip spacing between the ionophoretic microelectrode and the TMA-ISM, and a reduced pulse current. Another technical caveat is that activated TMA^+-permeating channels and transporters (eg. nicotinergic, TRP and NMDA channels) during CSD, as well as the TMA-induced neuronal excitability and connexin effects, could increase the non-specific loss of TMA^+ (k') from the extracellular space during SD, which may produce an underestimate in the changes in ECS size (Neher and Lux 1972); however, the conclusions would not be altered because similar effects were seen in $AQP4^{+/+}$ and $AQP4^{-/-}$ mice.

We conclude that baseline ECS expansion and reduced astrocyte water permeability are necessary and sufficient to account for the experimental observations. This conclusion is supported by studies in hippocampal slices showing that direct ECS expansion with hypertonic saline impairs hypoxia-induced spreading depression (Huang et al. 1996; Mane and Muller 2012), and that ECS contraction with hypotonic saline increases susceptibility to spreading depression (Chebabo et al. 1995). The reason(s) for baseline ECS expansion in $AQP4^{-/-}$ mice are not known, and so it is not possible to extrapolate data here to acute AQP4 inhibition without ECS expansion, as might occur with pharmacological inhibition of AQP4 in humans, if and when suitable AQP4-selective inhibitors become available. Mathematical modeling qualitatively reproduced our results but was not quantitatively accurate, suggesting that additional factors, such as Na^+, Cl^-, HCO_3^- and Ca^{2+} fluxes, synaptic glutamate release and electro-diffusion in the intracellular or extracellular space, also contribute to the velocity of CSD propagation.

In summary, we found that the rate of spreading depression propagation and the susceptibility to spreading depression is decreased in $AQP4^{-/-}$ mice, despite the expected reduction in extracellular K^+ clearance rate. These results extend prior findings demonstrating the role of AQP4 in cortical excitability and suggest that AQP4 increases susceptibility to CSD-related phenomena including migraine aura and anoxic depolarization following ischemia.

Acknowledgments

This work was supported by grants EB00415, NS50173, EY13574, DK35124, DK43840 and DK72517 from the National Institutes of Health, a grant from the Guthy-Jackson Charitable Foundation, and the UCSF Brain and Spinal Injury Center. We thank professors Charles Nicholson and Sabina Hrabetova for suggestions on TMA^+ measurements and data analysis, and Bas-Jan Zandt for providing Matlab code for CSD simulations.

References

Amiry-Moghaddam M, Frydenlund DS, Ottersen OP. Anchoring of aquaporin-4 in brain: molecular mechanisms and implications for the physiology and pathophysiology of water transport. Neuroscience. 2004; 129:999–1010. [PubMed: 15561415]

Amiry-Moghaddam M, Williamson A, Palomba M, Eid T, de Lanerolle NC, Nagelhus EA, Adams ME, Froehner SC, Agre P, Ottersen OP. Delayed K+ clearance associated with aquaporin-4 mislocalization: phenotypic defects in brains of alpha-syntrophin-null mice. Proc Natl Acad Sci U S A. 2003; 100:13615–20. [PubMed: 14597704]

Binder DK, Oshio K, Ma T, Verkman AS, Manley GT. Increased seizure threshold in mice lacking aquaporin-4 water channels. Neuroreport. 2004; 15:259–62. [PubMed: 15076748]

Binder DK, Yao X, Zador Z, Sick TJ, Verkman AS, Manley GT. Increased seizure duration and slowed potassium kinetics in mice lacking aquaporin-4 water channels. Glia. 2006; 53:631–6. [PubMed: 16470808]

Chebabo SR, Hester MA, Aitken PG, Somjen GG. Hypotonic exposure enhances synaptic transmission and triggers spreading depression in rat hippocampal tissue slices. Brain Res. 1995; 695:203–16. [PubMed: 8556332]

Connors NC, Adams ME, Froehner SC, Kofuji P. The potassium channel Kir4.1 associates with the dystrophin-glycoprotein complex via alpha-syntrophin in glia. J Biol Chem. 2004; 279:28387–92. [PubMed: 15102837]

Connors NC, Kofuji P. Potassium channel Kir4.1 macromolecular complex in retinal glial cells. Glia. 2006; 53:124–31. [PubMed: 16206160]

Dietzel I, Heinemann U, Hofmeier G, Lux HD. Transient changes in the size of the extracellular space in the sensorimotor cortex of cats in relation to stimulus-induced changes in potassium concentration. Exp Brain Res. 1980; 40:432–9. [PubMed: 6254790]

Frigeri A, Gropper MA, Turck CW, Verkman AS. Immunolocalization of the mercurial-insensitive water channel and glycerol intrinsic protein in epithelial cell plasma membranes. Proc Natl Acad Sci U S A. 1995; 92:4328–31. [PubMed: 7538665]

Godukhin OV, Obrenovitch TP. Asymmetric propagation of spreading depression along the anteroposterior axis of the cerebral cortex in mice. J Neurophysiol. 2001; 86:2109–11. [PubMed: 11600666]

Grafstein B. Mechanism of spreading cortical depression. J Neurophysiol. 1956; 19:154–71. [PubMed: 13295838]

Guedes RC, Barreto JM. Effect of anesthesia on the propagation of cortical spreading depression in rats. Braz J Med Biol Res. 1992; 25:393–7. [PubMed: 1342216]

Haj-Yasein NN, Jensen V, Ostby I, Omholt SW, Voipio J, Kaila K, Ottersen OP, Hvalby O, Nagelhus EA. Aquaporin-4 regulates extracellular space volume dynamics during high-frequency synaptic stimulation: a gene deletion study in mouse hippocampus. Glia. 2012; 60:867–74. [PubMed: 22419561]

Hansen AJ, Olsen CE. Brain extracellular space during spreading depression and ischemia. Acta Physiol Scand. 1980; 108:355–65. [PubMed: 7415848]

Hrabětová, S.; Nicholson, C. Biophysical properties of brain extracellular space explored with ion-selective microelectrodes, integrative optical imaging and related techniques. In: Michael, ACBL., editor. Electrochemical Methods for Neuroscience. Boca Raton: CRC Press, Taylor Francis Group; 2007. p. 167-204.

Huang R, Aitken PG, Somjen GG. Hypertonic environment prevents depolarization and improves functional recovery from hypoxia in hippocampal slices. J Cereb Blood Flow Metab. 1996; 16:462–7. [PubMed: 8621750]

Jin BJ, Zhang H, Binder DK, Verkman AS. Aquaporin-4-dependent K(+) and water transport modeled in brain extracellular space following neuroexcitation. J Gen Physiol. 2013; 141:119–32. [PubMed: 23277478]

Jing J, Aitken PG, Somjen GG. Interstitial volume changes during spreading depression (SD) and SD-like hypoxic depolarization in hippocampal tissue slices. J Neurophysiol. 1994; 71:2548–51. [PubMed: 7523614]

Kofuji P, Newman EA. Potassium buffering in the central nervous system. Neuroscience. 2004; 129:1045–56. [PubMed: 15561419]

Kume-Kick J, Mazel T, Vorisek I, Hrabetova S, Tao L, Nicholson C. Independence of extracellular tortuosity and volume fraction during osmotic challenge in rat neocortex. J Physiol. 2002; 542:515–27. [PubMed: 12122149]

Leao AAP. Spreading depression of activity in the cerebral cortex. J Neurophysiol. 1944; 7:359–390.

Lehmenkuhler A, Sykova E, Svoboda J, Zilles K, Nicholson C. Extracellular space parameters in the rat neocortex and subcortical white matter during postnatal development determined by diffusion analysis. Neuroscience. 1993; 55:339–51. [PubMed: 8377929]

Li J, Patil RV, Verkman AS. Mildly abnormal retinal function in transgenic mice without Muller cell aquaporin-4 water channels. Invest Ophthalmol Vis Sci. 2002; 43:573–9. [PubMed: 11818406]

Li J, Verkman AS. Impaired hearing in mice lacking aquaporin-4 water channels. J Biol Chem. 2001; 276:31233–7. [PubMed: 11406631]

Lu DC, Zhang H, Zador Z, Verkman AS. Impaired olfaction in mice lacking aquaporin-4 water channels. Faseb J. 2008; 22:3216–23. [PubMed: 18511552]

Ma T, Yang B, Gillespie A, Carlson EJ, Epstein CJ, Verkman AS. Generation and phenotype of a transgenic knockout mouse lacking the mercurial-insensitive water channel aquaporin-4. J Clin Invest. 1997; 100:957–62. [PubMed: 9276712]

Mane M, Muller M. Temporo-spectral imaging of intrinsic optical signals during hypoxia-induced spreading depression-like depolarization. PLoS One. 2012; 7:e43981. [PubMed: 22952835]

Manley GT, Fujimura M, Ma T, Noshita N, Filiz F, Bollen AW, Chan P, Verkman AS. Aquaporin-4 deletion in mice reduces brain edema after acute water intoxication and ischemic stroke. Nat Med. 2000; 6:159–63. [PubMed: 10655103]

Martins-Ferreira H, Ribeiro LJ. Biphasic effects of gap junctional uncoupling agents on the propagation of retinal spreading depression. Braz J Med Biol Res. 1995; 28:991–4. [PubMed: 8580888]

Mazel T, Richter F, Vargova L, Sykova E. Changes in extracellular space volume and geometry induced by cortical spreading depression in immature and adult rats. Physiol Res. 2002; 51(Suppl 1):S85–93. [PubMed: 12479789]

Miura RM, Huang H, Wylie JJ. Mathematical approaches to modeling of cortical spreading depression. Chaos. 2013; 23:046103. [PubMed: 24387582]

Nagelhus EA, Horio Y, Inanobe A, Fujita A, Haug FM, Nielsen S, Kurachi Y, Ottersen OP. Immunogold evidence suggests that coupling of K+ siphoning and water transport in rat retinal Muller cells is mediated by a coenrichment of Kir4.1 and AQP4 in specific membrane domains. Glia. 1999; 26:47–54. [PubMed: 10088671]

Nedergaard M, Cooper AJ, Goldman SA. Gap junctions are required for the propagation of spreading depression. J Neurobiol. 1995; 28:433–44. [PubMed: 8592104]

Neely JD, Amiry-Moghaddam M, Ottersen OP, Froehner SC, Agre P, Adams ME. Syntrophin-dependent expression and localization of Aquaporin-4 water channel protein. Proc Natl Acad Sci U S A. 2001; 98:14108–13. [PubMed: 11717465]

Neher E, Lux HD. Differential action of TEA + on two K +-current componentss of a molluscan neurone. Pflugers Arch. 1972; 336:87–100. [PubMed: 4673460]

Neher E, Lux HD. Rapid changes of potassium concentration at the outer surface of exposed single neurons during membrane current flow. J Gen Physiol. 1973; 61:385–99. [PubMed: 4689624]

Nicholson C. Ion-selective microelectrodes and diffusion measurements as tools to explore the brain cell microenvironment. J Neurosci Methods. 1993; 48:199–213. [PubMed: 8412303]

Nicholson C, Phillips JM. Ion diffusion modified by tortuosity and volume fraction in the extracellular microenvironment of the rat cerebellum. J Physiol. 1981; 321:225–57. [PubMed: 7338810]

Nielsen S, Nagelhus EA, Amiry-Moghaddam M, Bourque C, Agre P, Ottersen OP. Specialized membrane domains for water transport in glial cells: high-resolution immunogold cytochemistry of aquaporin-4 in rat brain. J Neurosci. 1997; 17:171–80. [PubMed: 8987746]

Oshio K, Binder DK, Yang B, Schecter S, Verkman AS, Manley GT. Expression of aquaporin water channels in mouse spinal cord. Neuroscience. 2004; 127:685–93. [PubMed: 15283967]

Padmawar P, Yao X, Bloch O, Manley GT, Verkman AS. K+ waves in brain cortex visualized using a long-wavelength K+-sensing fluorescent indicator. Nat Methods. 2005; 2:825–7. [PubMed: 16278651]

Papadopoulos MC, Manley GT, Krishna S, Verkman AS. Aquaporin-4 facilitates reabsorption of excess fluid in vasogenic brain edema. FASEB J. 2004; 18:1291–3. [PubMed: 15208268]

Papadopoulos MC, Verkman AS. Aquaporin-4 gene disruption in mice reduces brain swelling and mortality in pneumococcal meningitis. J Biol Chem. 2005; 280:13906–12. [PubMed: 15695511]

Papadopoulos MC, Verkman AS. Aquaporin water channels in the nervous system. Nat Rev Neurosci. 2013; 14:265–77. [PubMed: 23481483]

Pietrobon D, Moskowitz MA. Chaos and commotion in the wake of cortical spreading depression and spreading depolarizations. Nat Rev Neurosci. 2014; 15:379–93. [PubMed: 24857965]

Prince DA, Lux HD, Neher E. Measurement of extracellular potassium activity in cat cortex. Brain Res. 1973; 50:489–95. [PubMed: 4705519]

Ruiz-Ederra J, Zhang H, Verkman AS. Evidence against functional interaction between aquaporin-4 water channels and Kir4.1 potassium channels in retinal Muller cells. J Biol Chem. 2007; 282:21866–72. [PubMed: 17525153]

Solenov E, Watanabe H, Manley GT, Verkman AS. Sevenfold-reduced osmotic water permeability in primary astrocyte cultures from AQP-4-deficient mice, measured by a fluorescence quenching method. Am J Physiol Cell Physiol. 2004; 286:C426–32. [PubMed: 14576087]

Somjen GG. Mechanisms of spreading depression and hypoxic spreading depression-like depolarization. Physiol Rev. 2001; 81:1065–96. [PubMed: 11427692]

Strohschein S, Huttmann K, Gabriel S, Binder DK, Heinemann U, Steinhauser C. Impact of aquaporin-4 channels on K+ buffering and gap junction coupling in the hippocampus. Glia. 2011; 59:973–80. [PubMed: 21446052]

Sykova E, Nicholson C. Diffusion in brain extracellular space. Physiol Rev. 2008; 88:1277–340. [PubMed: 18923183]

Tamura K, Alessandri B, Heimann A, Kempski O. The effect of a gap-junction blocker, carbenoxolone, on ischemic brain injury and cortical spreading depression. Neuroscience. 2011; 194:262–71. [PubMed: 21839806]

Theis M, Jauch R, Zhuo L, Speidel D, Wallraff A, Doring B, Frisch C, Sohl G, Teubner B, Euwens C, et al. Accelerated hippocampal spreading depression and enhanced locomotory activity in mice with astrocyte-directed inactivation of connexin43. J Neurosci. 2003; 23:766–76. [PubMed: 12574405]

Thiagarajah JR, Papadopoulos MC, Verkman AS. Noninvasive early detection of brain edema in mice by near-infrared light scattering. J Neurosci Res. 2005; 80:293–9. [PubMed: 15765520]

Thrane AS, Takano T, Rangroo Thrane V, Wang F, Peng W, Ottersen OP, Nedergaard M, Nagelhus EA. In vivo NADH fluorescence imaging indicates effect of aquaporin-4 deletion on oxygen microdistribution in cortical spreading depression. J Cereb Blood Flow Metab. 2013; 33:996–9. [PubMed: 23611872]

Xie L, Kang H, Xu Q, Chen MJ, Liao Y, Thiyagarajan M, O'Donnell J, Christensen DJ, Nicholson C, Iliff JJ, et al. Sleep drives metabolite clearance from the adult brain. Science. 2013; 342:373–7. [PubMed: 24136970]

Yao X, Hrabetova S, Nicholson C, Manley GT. Aquaporin-4-deficient mice have increased extracellular space without tortuosity change. J Neurosci. 2008; 28:5460–4. [PubMed: 18495879]

Zandt BJ, ten Haken B, van Putten MJ. Diffusing substances during spreading depolarization: analytical expressions for propagation speed, triggering, and concentration time courses. J Neurosci. 2013; 33:5915–23. [PubMed: 23554473]

Zhang H, Verkman AS. Aquaporin-4 independent Kir4.1 K(+) channel function in brain glial cells. Mol Cell Neurosci. 2007

Main Points

- The velocity and frequency of CSD depolarizations were significantly reduced in AQP4$^{-/-}$ mice compared to AQP4$^{+/+}$ mice.
- The kinetics of increase in extracellular space K^+ during CSD and the clearance of K^+ following CSD were significantly reduced in AQP4$^{-/-}$ mice.
- ECS volume fraction was greatly reduced during CSD depolarizations.
- Mathematical modeling showed that reduced velocity of CSD propagation in AQP4$^{-/-}$ mice was a consequence of the slowed increase in extracellular space K^+ during neuronal depolarization.

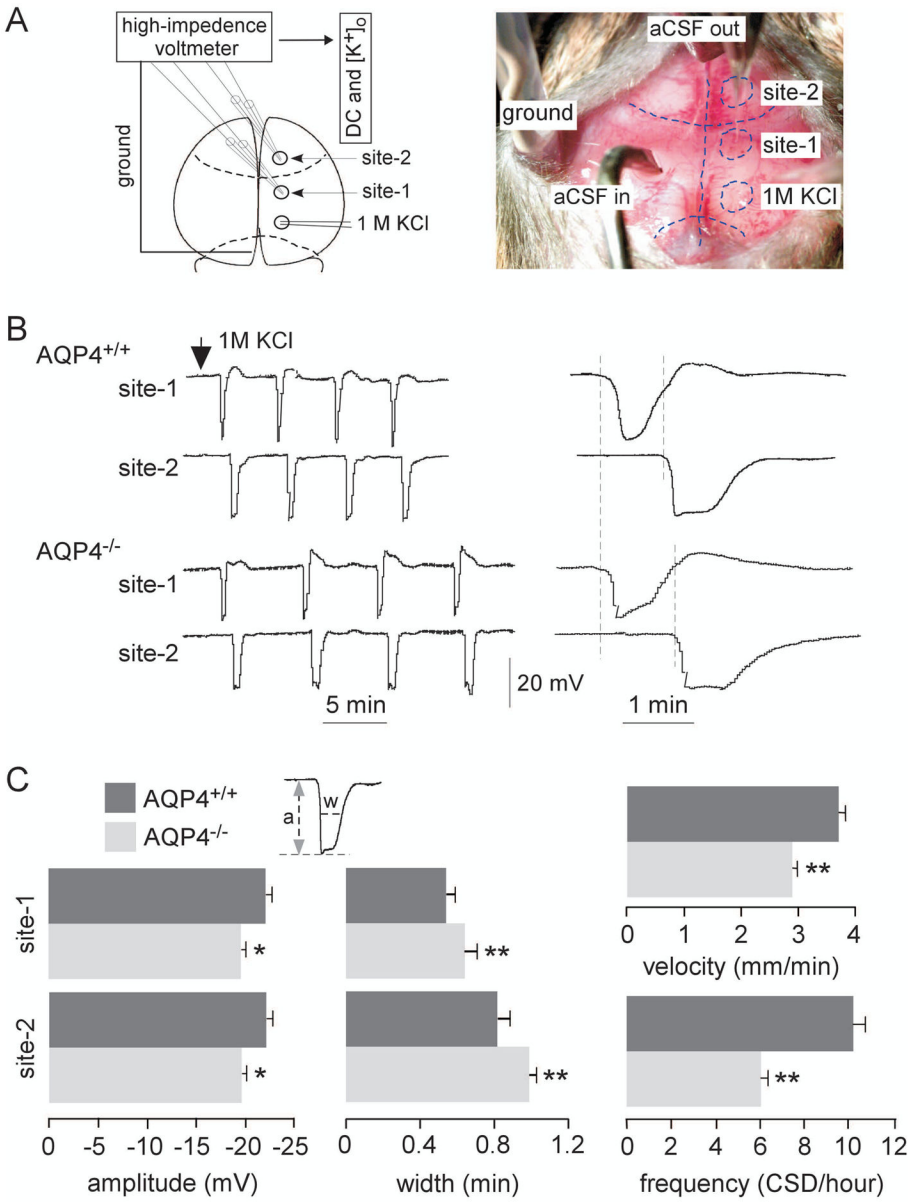

Figure 1.

In vivo recording of direct current (DC) potentials during cortical spreading depression (CSD) induced by KCl infusion. **A.** Experimental set-up showing DC potentials monitored at site-1 and site-2. CSD was produced by continuous application of 1M KCl. **B.** Representative DC potentials during CSD from $AQP4^{+/+}$ and $AQP4^{-/-}$ mice. Arrow denotes the initiation of 1M KCl application. The right panel shows time-expanded curves, with dashed vertical lines showing delay in onset of depolarizations from which propagation velocity was determined. **C.** Amplitude, width (at half-maximum), propagation velocity and frequency in $AQP4^{+/+}$ and $AQP4^{-/-}$ mice (8 per group) during CSD (mean ± SEM, * $p < 0.05$, ** $p < 0.01$).

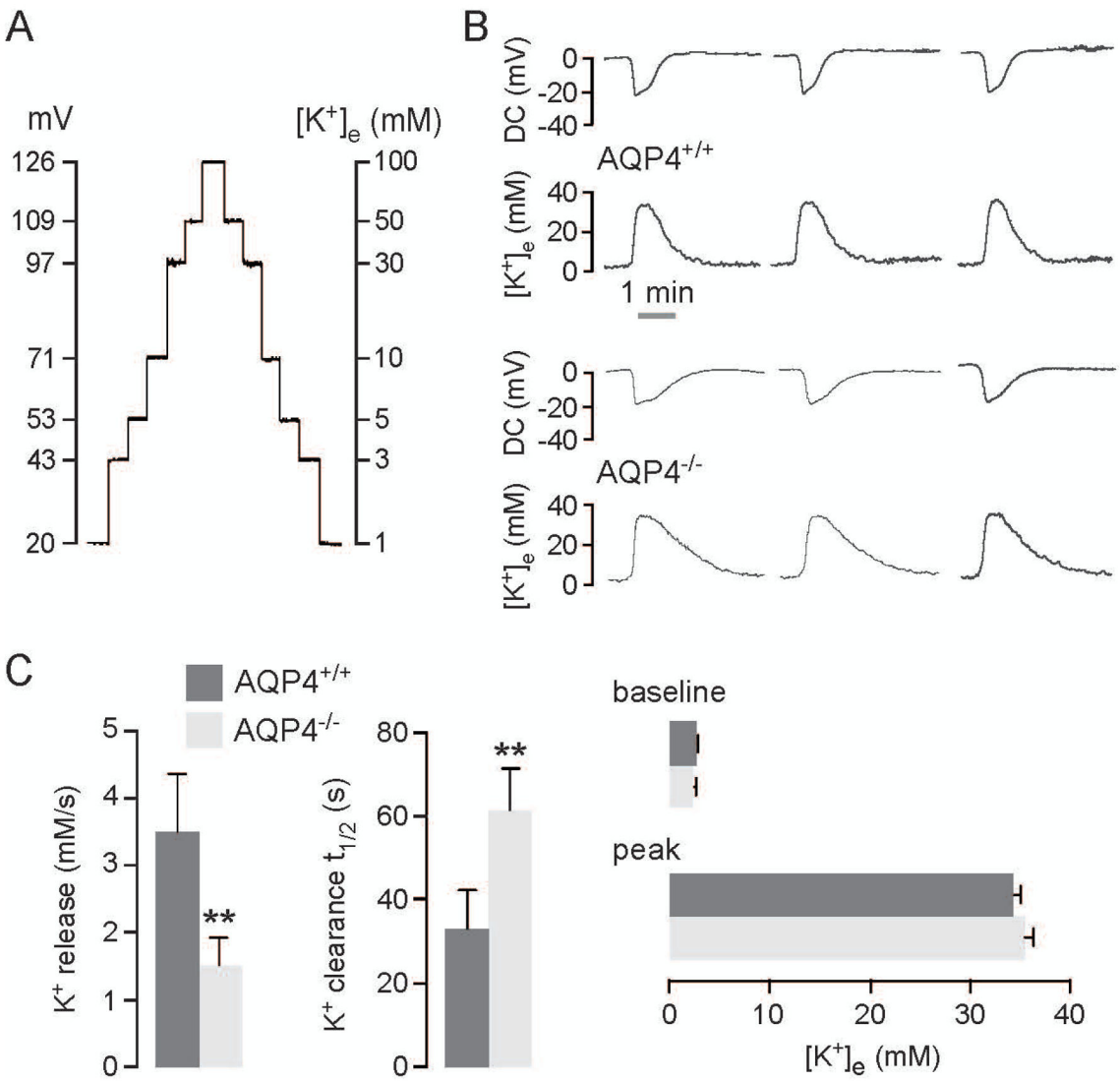

Figure 2.

In vivo recording of extracellular space K^+ concentration during CSD. **A.** Calibration curve for K^+-sensitive microelectrode using K^+ solution standards containing 1, 3, 5, 10, 30, 50 and 100 mM KCl. Calibrations were done for the same microelectrode before and after each *in vivo* measurement. **B.** CSD was induced as in Fig. 1A. Representative K^+ and DC potential recordings from three AQP4$^{+/+}$ and AQP4$^{-/-}$ mice. **C.** (left) Rate (in mM/s) of increase in K^+ increase (K^+ release), and exponential time constant (in s^{-1}) for K^+ recovery to baseline (K^+ clearance). (right) Baseline and peak K^+ concentrations. Data shown for 6 mice per group (mean ± SEM, ** $p < 0.01$).

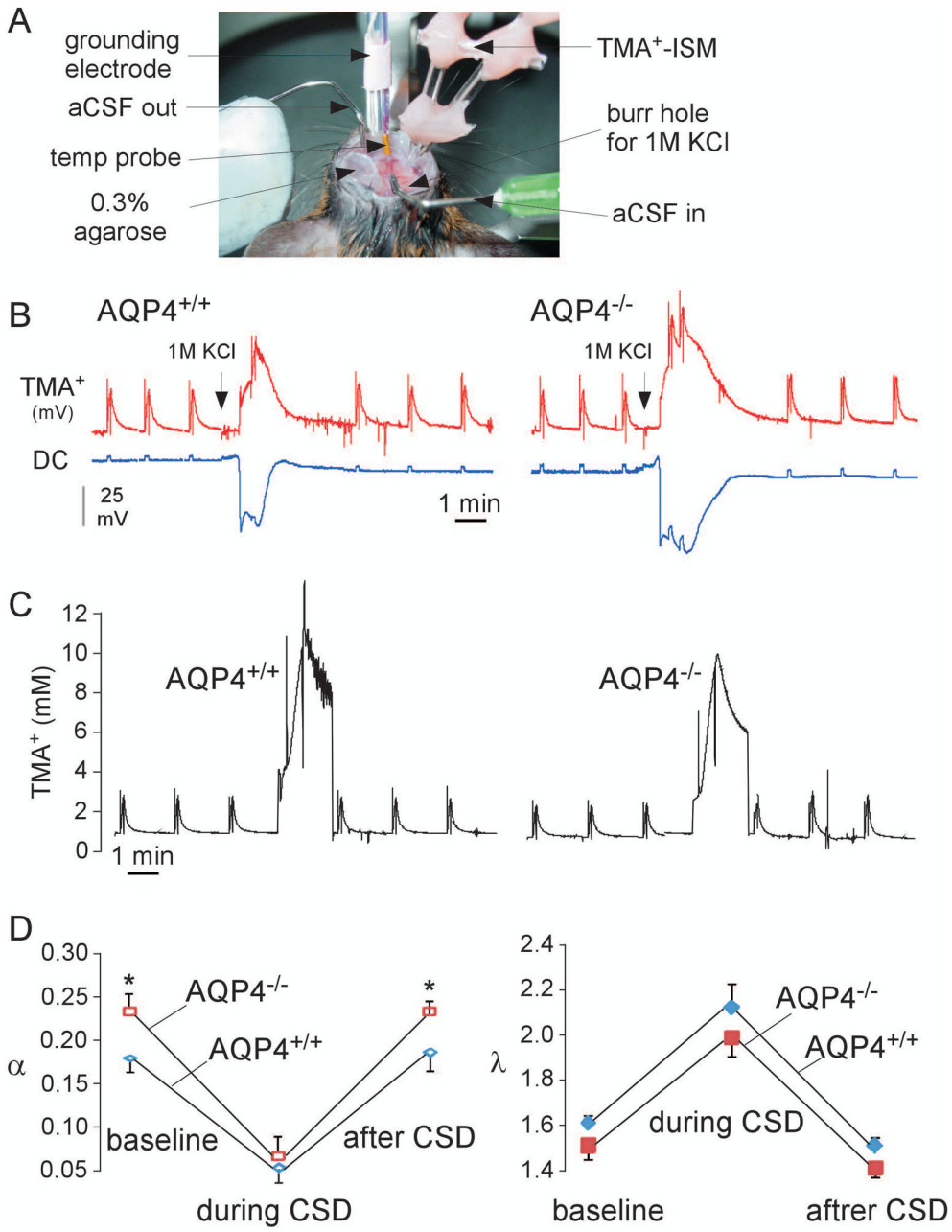

Figure 3.

In vivo measurement of ECS volume and tortuosity during CSD. **A.** Experimental setup for TMA^+ diffusion measurements showing the immobilized mouse head and an array of microelectrodes with fixed inter-tip distance, adjacent to a grounding electrode and a temperature probe. **B.** Representative original recordings from TMA^+-sensitive microelectrode and DC potential. Spikes initiated by 4 s-pulsed iontophoresis of TMA^+. **C.** Deduced kinetics of TMA^+ concentration from curves in B. A non-zero concentration of TMA^+ in brain tissue was maintained by continuous application of a small bias current (20

nA). **D.** Averaged ECS volume fraction (α) and tortuosity (λ) (mean ± SEM, 4 mice per group, *$p < 0.05$).

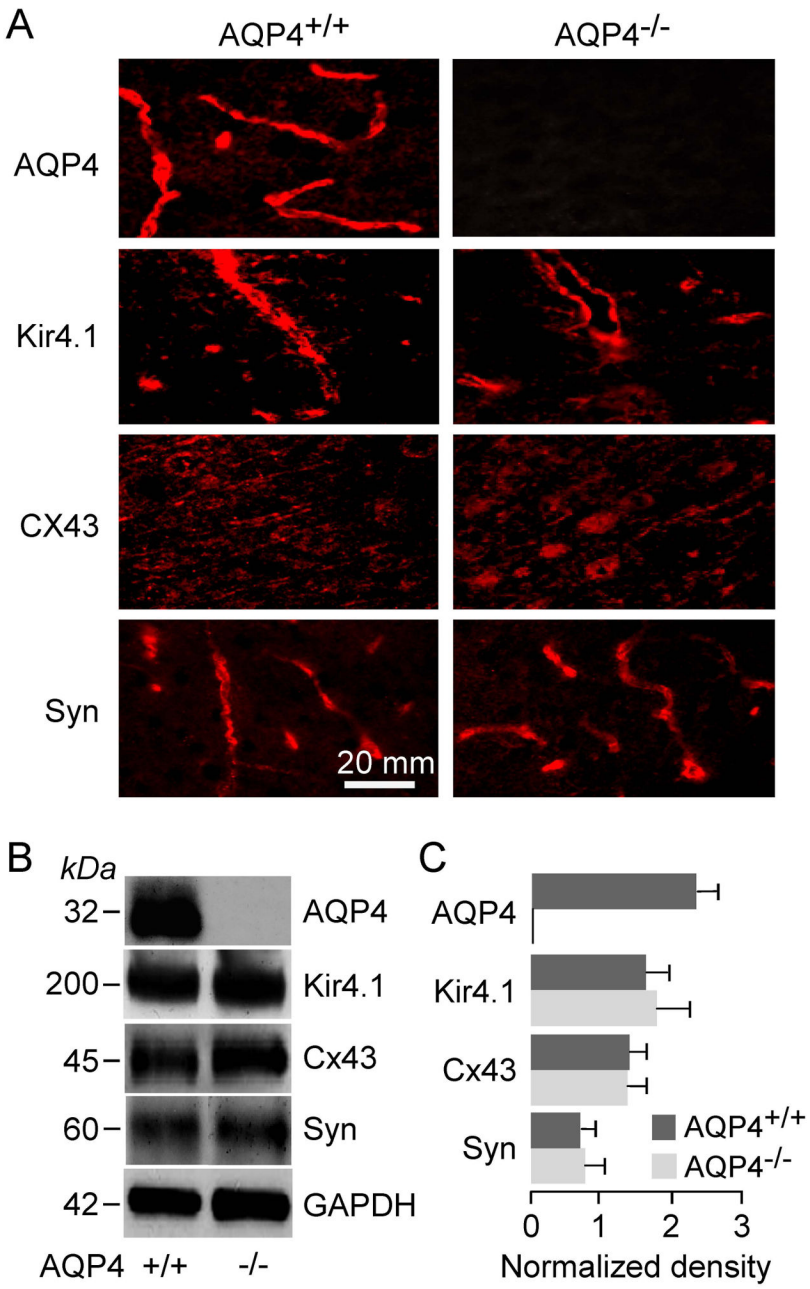

Figure 4.

Expression of AQP4, Kir4.1, Cx43, and α-syntrophin in membrane homogenates of brain cortex of AQP4$^{+/+}$ and AQP4$^{-/-}$ mice. **A**. Immunofluorescence using specific antibodies. **B**. Immunoblot with GAPDH as internal control. **C.** Kir4.1, α-syntrophin and Cx43 protein quantified by densitometry normalized to GAPDH expression (3 mice per group, mean ± SEM, differences not significant).

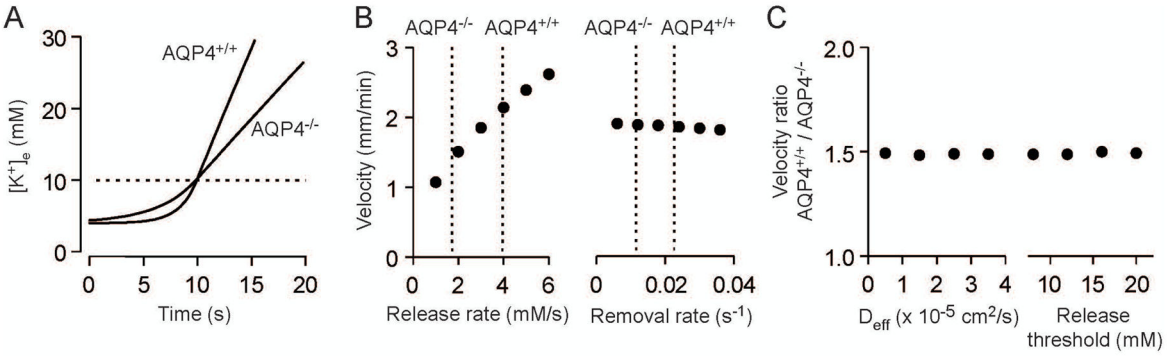

Figure 5.

Modeling predicts slower propagation of spreading depression in AQP4$^{-/-}$ mice. **A.** $[K^+]_e$ changes during the initial phase of CSD were modelled as described by Zandt et al. (Zandt et al. 2013) using experimentally determined values for K^+ release rate (AQP4$^{+/+}$ 3.95 mM/s, AQP4$^{-/-}$ 1.72 mM/s), reuptake rate constant (AQP4$^{+/+}$ 0.0226 s^{-1}, AQP4$^{-/-}$ 0.0116 s^{-1}) and effective diffusion coefficient (AQP4$^{+/+}$ 0.796 × 10^{-5} cm^2/s, AQP4$^{-/-}$ 0.907 × 10^{-5} cm^2/s). Neuronal K^+ release threshold was set at 10 mM (dotted line). **B.** Dependence of CSD propagation velocity on rates of K^+ release rate and removal modelled for a neuronal release threshold of 10 mM K^+ and effective K^+ diffusion coefficient of 2 × 10^{-5} cm^2/s. Dotted lines denote experimentally measured release and removal rates in AQP4$^{+/+}$ and AQP4$^{-/-}$ mice. **C.** Dependence of relative CSD propagation velocity on K^+ diffusion coefficient and the threshold for neuronal K^+ release.

Table 1

ECS volume fraction (α), tortuosity (λ), and TMA^+ loss parameter (k′) in the somatosensory neocortex of $AQP4^{+/+}$ and $AQP4^{-/-}$ mice before, during and after CSD.

	before CSD	during CSD	30 min after CSD
$AQP4^{+/+}$			
α	0.18 ± 0.003	0.045 ± 0.005	0.19 ± 0.004
λ	1.61 ± 0.02	2.27 ± 0.15	1.64 ± 0.04
k′	0.0031 ± 0.0009	0.038 ± 0.005	0.0055 ± 0.0007
n	6	4	4
$AQP4^{-/-}$			
α	0.23 ± 0.007**	0.055 ± 0.003	0.24 ± 0.005
λ	1.62 ± 0.04	2.38 ± 0.21	1.68 ± 0.03
k′	0.0045 ± 0.0001	0.02718 ± 0.006	0.0038 ± 0.0002
n	6	4	4

Data are expressed as mean ± SEM with *n* mice per group.

** $P < 0.001$ (two- sample equal variance *t*-test) comparing $AQP4^{+/+}$ and $AQP4^{-/-}$ mice.